Journal of Thermal Analysis and Calorimetry (2024) 149:8579–8596
https://doi.org/10.1007/s10973-024-13209-1

Thermohydraulic performance of convergent and rectangular microchannels with rectangular grooves using silver nanofluid: numerical study

Nehad Abid Allah Hamza[1] · Isam Mejbel Abed[2] · Nejla Mahjoub Said[3]

Received: 31 January 2024 / Accepted: 10 April 2024 / Published online: 16 May 2024

Abstract

This study focuses on enhancing the performance of microchannel heat sinks (MCHSs) through the incorporation of longitudinal rectangular-sided grooves in conjunction with standard designs such as rectangular microchannels and converging microchannels. The aim is to improve hydrothermal properties, including fluid flow and the reduction in the pressure drop. The study explores the augmented heat transfer achieved by employing a higher-thermal-conductivity fluid along with the use of these grooves to disrupt the thermal boundary layer and induce secondary flow. Utilizing a 3D numerical model based on the finite element approach, investigations are conducted on a copper heat sink with slight variations in both hydraulic diameter and conjugated heated area. Silver/water nanofluid with different volume fraction values (0, 0.025, 0.05 and 0.075) is employed. Comparative analysis of pressure drops among conventional MCHS and other designs, namely rectangular with side rectangular grooves, converge (CMCHS) and converge with side rectangular grooves (CMCHS-WSRG) microchannel heat sinks, reveals that an increase in nanofluid volume concentration results in elevated pressure drop across all models. The design of RMCH and CMCHS without side rectangular grooves is shown to decrease the fluid flow pressure drop by 12.5 and 33.35%, respectively. Additionally, the study indicates that the average temperature of the heat sink base in CMCHS-WSRG is lower than in other designs. A comparison of the hydrothermal performance factor of the three models with the standard MCHS demonstrates that RMWSR grooves exhibit higher hydrothermal performance due to their larger conjugated heated area. The use of CMCHS-WSRG generates a higher velocity distribution compared to other designs. In conclusion, the incorporation of longitudinal rectangular grooves is found to enhance the hydrothermal performance of MCHS.

Keywords Hydrothermal performance · Nanofluids · Pressure drop · Nusselt number · Microchannel heat sink · Grooves

List of symbols

$A_{con.}$	Convection heat transfer area, m
c_p	Specific heat, J Kg^{-1} K^{-1}
D_h	Hydraulic diameter, m
h	Heat transfer coefficient, W m^{-2} K^{-1}
k	Thermal conductivity, W m^{-1} K^{-1}
L	Length of the microchannel heat sink, m
H_t	Total height of channel, m
Δp	Pressure drop, Pa
PEC	Performance evaluation criteria
q	Heat flux at the base of the heat sink, W m^{-2}
f	Friction factor
Re	Reynolds number
T	Temperature, K
W_c	Channel width, m

Greek symbols

ρ	Density, kg m^{-3}
μ	Dynamic viscosity, Ns m^{-2}

Subscripts

b	Bottom
nf	Nanofluid
ch	Channel
w	Wall
t	Top

✉ Nejla Mahjoub Said
nalmahjoub@kku.edu.sa

[1] College of Engineering, Al-Qasim Green University, Hillah, Babylon 51001, Iraq

[2] Mechanical Engineering Department, College of Engineering, University of Babylon, Hillah, Babylon 51001, Iraq

[3] Department of Physics, College of Science, King Khalid University, Abha 61413, Saudi Arabia

Abbreviations

MCHS	Microchannel heat sink
RMCHS	Rectangular microchannel heat sink
RMCH-WSRG	Rectangular microchannel heat sink with side rectangular groove
CMCHS	Converge microchannel heat sink
CMCH-WSRG	Converge microchannel heat sink with side rectangular groove
AEQ	Average equality
FV	Front view

Introduction

The increasing heat flux generated by electronic components requires effective heat dissipation for damage prevention and optimal performance. Microchannel heat sinks (MCHSs) have emerged as a practical solution to this challenge, finding applications in LED lighting and diverse thermal management scenarios [1]. Conventional cooling methods are proving inadequate as the demand rises for compact, high-performance electronic devices. Leveraging the distinctive heat transfer characteristics at the microscale, MCHS presents an appealing solution [2].

The hydrothermal performance of microchannels is affected by fluid parameters such as flow rate, thermal conductivity and dynamic viscosity. Additionally, factors like channel geometry, material thermal conductivity and surface roughness impact the overall performance of microchannel heat sinks [3]. Researchers have extensively explored flow and heat transfer characteristics in microchannels to enhance their thermal performance and optimize design. Studies have investigated the impact of different channel geometries and the use of diverse fluids with varying thermal properties to improve cooling efficiency. Notably, the use of nanofluids holds promise for smaller and lighter cooling systems, especially in micro- and nano-electro-mechanical systems (MEMS and NEMS) and devices utilizing lasers, optical fibers, fuel cells, etc. To fully exploit the heat transfer benefits offered by nanofluids, it is crucial to ensure the stability of nanoparticles, preventing issues such as clogging and sedimentation within heat transfer equipment [4].

Several studies have explored the effectiveness of different nanofluids in enhancing heat transfer in microchannels. For instance, Hung and Yan [5] investigated a double-layer microchannel with Al_2O_3 nanofluid, achieving a 26% increase in thermal performance. Ahmed et al. [6] conducted a numerical investigation on a wavy channel using copper–water nanofluid, identifying nanoparticle volume fraction, wavy wall amplitude and Reynolds number as key variables influencing heat transfer. Wang et al. [7] performed experimental work with Al_2O_3/H_2O nanofluid in a straight microchannel heat sink, achieving maximum heat transfer performance with a 4% volume nanofluid.

Praveen et al. [8] used fly ash as a nanofluid in the experimental work to determine the effect of this type of nanofluid on heat transfer and friction factor at a volume fraction of up to 2.0 vol %. The outcomes of this simulation show that the Nusselt number (Nu) is enhanced by 46.9% and there is a 9.89% increase in friction factor. Also, the fly ash with Cu as nanofluid was used by in the experimental work by Praveen, et al. [9] in the thermal engineering system. The results of this work showed the thermal performance enhanced with using this type of nanofluid, while the pressure drop became large. Many studies have shown that nanoparticle size can affect the hydrothermal performance of thermal management systems, and Praveen et al. [10] showed that using Al_2O_3 as a nanoparticle in size of 30 nm can enhance the hydrothermal performance compared with 50 nm and 80 nm.

Sivakumar et al. [11] conducted an experimental study on Al_2O_3–H_2O and CuO–H_2O nanofluids in a serpentine-shaped microchannel heat sink, demonstrating improved heat transfer coefficients with higher nanoparticle concentrations.

Rostami and Abbassi [12] employed Al_2O_3 nanofluids in a wavy microchannel, revealing increased Nusselt numbers with minimal changes in pressure drop. Anbumeenakshi and Thansekhar [13] investigated Al_2O_3/water nanofluids in a microchannel heat sink subjected to non-uniform heat flux, observing decreased average surface temperatures with increasing volume concentration.

Naphon et al. [14] carried out an experimental exploration into the effects of TiO_2 nanofluids on the heat transfer and flow characteristics within a microchannel heat sink. This investigation encompassed three heat transfer enhancement techniques: microchannel heat sinks, jet impingement and nanofluids. The results revealed a substantial 18.56% increase in convective heat transfer at a nanofluid concentration of 0.015%, underscoring the notable impact of incorporating nanoparticles into the base fluid. In a study by Ali et al. [15], both experimental and numerical approaches were employed to examine the influence of different heat sink designs and various flow rates of working fluids (CuO–H_2O and Al_2O_3–H_2O). The findings indicated that Al_2O_3–H_2O nanofluid exhibited superior heat transfer rates compared to distilled water and CuO–H_2O nanofluid. Additionally, an escalation in flow rate and the utilization of nanofluids led to a decrease in the base temperature.

Sajid et al. [16] conducted an experimental investigation into the heat transfer and hydrodynamic characteristics of TiO_2–H_2O nanofluid in heat sinks with wavy channels. The study explored diverse nanofluid concentrations, emphasizing the superior heat transfer characteristics of nanofluids compared to distilled water. Balaji et al. [17] employed functionalized graphene nanoplatelets (GnP) in distilled water to enhance thermal conductivity in a microchannel

heat sink. Their research delved into various heat transport parameters, revealing a temperature reduction of 10 °C in the heat sink, along with substantial increases of 71% in the convective heat transfer coefficient and 60% in the Nusselt number, accompanied by only a 12% rise in pressure drop compared to water.

Bazdar et al. [18] executed a 3D numerical study on heat transfer and turbulent flow in a wavy microchannel using CuO–H_2O nanofluid. The investigation unveiled an increase in the Nusselt number when the Reynolds number surpassed 7500. Plant and Saghir [19] utilized different concentrations of Al_2O_3 in a straight microchannel heat sink with two and three channels, illustrating a maximum thermal enhancement of 24.5% for a 1% concentration of nanofluid compared to 2%. Heidarshenas et al. [20] conducted experimental research on the effect of various alumina nanoparticle sizes on forced convection heat transfer in a cylindrical microchannel heat sink. Larger particle sizes resulted in reduced heat transfer coefficients, significantly affecting the Nusselt number.

Nimmagadda [21] explored the heat transfer enhancement of an Al_2O_3/silver hybrid nanofluid in a rectangular microchannel, resulting in a significant increase in the convective heat transfer coefficient.

There is another alternative method to simulate heat transfer in a microchannel heat sink. One of these methods is the lattice Boltzmann method which can be employed in various applications such as in radiation simulation [22, 23] and moving boundary simulation [24].

All the above studies are related to using the passive technique for enhancement heat transfer in MCHS. Active techniques are another method that allows for the improvement of thermal performance, and one of these techniques is ultrasonic vibration. Delouei et al. [25] studied experimentally using ultrasonic vibration to enhance the cooling efficiency in an electronic system, and the findings showed that this technique can highly increase the cooling efficiency of the computers where the highest improvement reached 20.687% at a low volume flow rate. Delouei et al. [26] used this technique in the experimental work related to enhancing thermal efficiency in indirect water bath heaters, and the findings showed that ultrasonic vibration can increase the heat transfer at a low flow rate.

It can be concluded from the above literature survey that previous studies focused on heat transfer enhancement with optimization of the geometry of MCHS by using many structures such as multiple ribs, dimples and cavities with multiple shapes, and such structure becomes more complex in the fabrication process. Hence, it is necessary to explore a new model that is easy in the fabrication process with higher heat transfer performance and low pressure drop. The new models can be considered the development of the traditional shape of MCHS which has a rectangular cross-sectional area. On the other hand, the literature review showed that oxide nanofluids have been extensively examined in various microchannel configurations to enhance microchannel heat sink performance. So, the current work aims to contribute to this research by presenting a numerical study that analyzes the hydrothermal performance (pressure drop and heat transfer) of Silver/water which has higher thermal conductivity as a cooling liquid in microchannels with new designs, specifically rectangular microchannels with side rectangular grooves (RMCHS-WSRG) and converging microchannels with side rectangular grooves (CMCH-WSRG). This innovative design incorporates longitudinal rectangular grooves on both sides of RMCHS and CMCHS, addressing the limited studies on the effect of rectangular grooves on enhancing hydrothermal performance. The innovative design that included grooves along the two sided of RMCH and CMCH can enhance the heat transfer without needing external energy consumption, so these designs are based on passive technique. Also, these grooves can generate fluid flow across the two sides of MCHS that possess temperature gradients, hence leading to enhanced thermal efficiency of the electronic system. On the other side, using CMCH can rise thermal performance by decreasing the hydraulic diameter that can cause to the increase the velocity of fluid flow.

Mathematical analysis

Assumptions

The following assumptions are used to solve the governing equations

(1) Fluid flow is steady and incompressible, and laminar flow.
(2) Neglect the heat transfer by radiation and thermal contact resistance between components;
(3) The properties of solid and fluid domains are constant;
(4) Neglect both gravitational force and viscous dissipation.

Governing equations

Based on the above assumptions, the governing equations include conservation of mass (continuity), momentum and energy for liquid and besides the energy equation for a solid domain, as explained below.

Continuity equation for the fluid (a coolant) [27]

$$\frac{\partial u}{\partial x}+\frac{\partial v}{\partial y}+\frac{\partial w}{\partial z}=0 \tag{1}$$

Momentum equations in 3D, for the nanofluid [27]

$$\frac{\partial u}{\partial x}+v\frac{\partial u}{\partial y}+w\frac{\partial u}{\partial z}=-\frac{1}{\rho_{\mathrm{nf}}}\frac{\partial p}{\partial x}+\frac{\mu_{\mathrm{nf}}}{\rho_{\mathrm{nf}}}\left(\frac{\partial^2 u}{\partial x^2}+\frac{\partial^2 u}{\partial y^2}+\frac{\partial^2 u}{\partial z^2}\right) \tag{2a}$$

$$\frac{\partial v}{\partial x}+v\frac{\partial v}{\partial y}+w\frac{\partial v}{\partial z}=-\frac{1}{\rho_{\mathrm{nf}}}\frac{\partial p}{\partial y}+\frac{\mu_{\mathrm{nf}}}{\rho_{\mathrm{nf}}}\left(\frac{\partial^2 v}{\partial x^2}+\frac{\partial^2 v}{\partial y^2}+\frac{\partial^2 v}{\partial z^2}\right) \tag{2b}$$

$$\frac{\partial w}{\partial x}+v\frac{\partial w}{\partial y}+w\frac{\partial w}{\partial z}=-\frac{1}{\rho_{\mathrm{nf}}}\frac{\partial p}{\partial z}+\frac{\mu_{\mathrm{nf}}}{\rho_{\mathrm{nf}}}\left(\frac{\partial^2 w}{\partial x^2}+\frac{\partial^2 w}{\partial y^2}+\frac{\partial^2 w}{\partial z^2}\right) \tag{2c}$$

Equations (2a), (2b) and (2c) are in the x, y and z directions only.

Energy equation of nanofluid [27]

$$u\frac{\partial T_{\mathrm{f}}}{\partial x}+v\frac{\partial T_{\mathrm{f}}}{\partial y}+w\frac{\partial T_{\mathrm{f}}}{\partial z}=\frac{k_{\mathrm{nf}}}{\rho_{\mathrm{nf}}cp_{\mathrm{nf}}}\left(\frac{\partial^2 T_{\mathrm{f}}}{\partial x^2}+\frac{\partial^2 T_{\mathrm{f}}}{\partial y^2}+\frac{\partial^2 T_{\mathrm{f}}}{\partial z^2}\right) \tag{3}$$

The above equations are applied when nanofluid is used as the coolant, if the liquid is water the subscript (nf) change (*f*).

Energy equation of solid domain

$$\left(\frac{\partial^2 Ts}{\partial x^2}+\frac{\partial^2 Ts}{\partial y^2}+\frac{\partial^2 Ts}{\partial z^2}\right)=0 \tag{4}$$

The physical properties that are used in the governing equations are more important because the hydraulic performance of the microchannel is affected by it. Nanofluid viscosity and effective density are effects on the pumping power of nanofluid in the microchannel, so the values of these properties which are limited by the type of nanofluid must be taken into consideration. Equation (5) is used to calculate the viscosity of nanofluid [28].

$$\mu_{\mathrm{nf}}=\mu_{\mathrm{bf}}(1+2.5\varphi) \tag{5}$$

The effective density of the nanofluids containing suspended particles can be evaluated by the following equation [28].

$$\rho_{\mathrm{nf}}=(1-\varphi)\rho_{\mathrm{bf}}+\varphi\rho_{\mathrm{P}} \tag{6}$$

where ϕ is the nanoparticle volume fraction and, μ_{bf}, ρ_{bf} are the dynamic viscosity and density of basic fluid, respectively. Water with thermal conductivity of 0.613 W m^{-1} °C^{-1} is used as basic fluid due to its relatively high thermal conductivity compared to other types of basic fluid.

On the other side, the thermal performance of MCHS is affected as mentioned next by thermal conductivity, specific heat and effective thermal diffusivity of coolant liquids besides viscosity and density, so the thermal conductivity of nanofluid can be calculated using Eq. (7) [28].

$$\frac{k_{\mathrm{nf}}}{k_{\mathrm{bf}}}=\frac{k_{\mathrm{p}}+2k_{\mathrm{bf}}+2(k_{\mathrm{pf}}-k_{\mathrm{p}})\varphi}{k_{\mathrm{p}}+2k_{\mathrm{bf}}-(k_{\mathrm{bf}}-k_{\mathrm{p}})\varphi} \tag{7}$$

Effective specific heat of nanofluids can be calculated using Eq. (8) [29]

$$c_{p_{\mathrm{nf}}}=\varphi\left(c_{\mathrm{p}}\right)_{\mathrm{P}}+(1-\varphi)\left(c_{\mathrm{p}}\right)_{\mathrm{bf}} \tag{8}$$

Thermal diffusivity of nanofluids calculated using Eq. (9) [29]

$$\alpha_{\mathrm{nf}}=\frac{k_{\mathrm{nf}}}{(1-\varphi)\left(\rho c_{\mathrm{p}}\right)_{\mathrm{bf}}+\varphi\left(\rho c_{\mathrm{p}}\right)_{\mathrm{p}}} \tag{9}$$

Data reduction

The related expressions for investigating the hydrothermal performance in MCHS are listed below:

The pressure drop (Δp) between the entry and exit of microchannel heat sink is calculated from Eq. (10)

$$\Delta p=p_{\mathrm{in}}-p_{\mathrm{out}} \tag{10}$$

p_{in} and p_{out} are the average pressure at the inlet and exit of the microchannel. Equations (11–14) are very important due to several parameters calculated from it [30]

$$D_{\mathrm{h}}=\frac{2H_{\mathrm{c}}W_{\mathrm{c}}}{H_{\mathrm{c}}+W_{\mathrm{c}}} \tag{11}$$

where D_{h} represents the hydraulic diameter and it is calculated as in Eq. (11). The Reynolds number (Re) is a dimensionless parameter used as a measure of fluid velocity, mass flow rate of fluid flow and type of fluid flow and is calculated by Eq. (12) [31]

$$\mathrm{Re}=\frac{\rho_{\mathrm{nf}}u_{\mathrm{m}}D_{\mathrm{h}}}{\mu_{\mathrm{nf}}} \tag{12}$$

The average Nusselt number is another important parameter for evaluating the convective heat transfer performance, which is defined as shown in Eq. (13) [32]

$$\mathrm{Nu}=\frac{\overline{h}D_{\mathrm{h}}}{k_{\mathrm{nf}}} \tag{13}$$

where k_{nf} is the thermal conductivity of the nanofluid and $\overline{h}$ is the average convective heat transfer coefficient, defined as follows [33],

$$h_{\text{ave}} = \frac{q_{\text{in}}\, \text{A}_{\text{b}}}{A_{\text{con.}}\left(T_{\text{b, aver}} - T_{f,\text{ ave}}\right)} \tag{14}$$

where $A_{\text{con.}}$, $T_{\text{b,ave}}$ and $T_{\text{f,ave}}$ are convection heat transfer area, average temperature of microchannel wall and average fluid temperature. The convection heat transfer area A_{con} is calculated concerning the geometry of the microchannel heat sink. $T_{\text{W,ave}}$ and $T_{\text{f,ave}}$ can be calculated numerically using Eqs. (15) and (16) [33].

$$T_{\text{b,ave}} = \frac{\int T\text{d}A}{\int \text{d}A} \tag{15}$$

$$T_{\text{f,ave}} = \frac{\int T\rho_{\text{nf}}\text{d}V}{\int \rho_{\text{nf}}\text{d}V} \tag{16}$$

To verify the heat transfer enhancement, an appropriate index called the Performance Evaluation Criterion (PEC) can be used, which is presented in Eq. (17) [34].

$$\text{PEc} = \left(\frac{\text{Nu New}}{\text{Nuo}}\right)/\left(\frac{f\text{New}}{fo}\right)^{1/3} \tag{17}$$

Computational domain

Geometry configurations

The numerical 3D model and the simulation of conjugate heat transfer involving heat transfer in solids and fluids, as well as laminar flow, were solved by COMSOL Multiphysics 6.0 that employs finite element (FEM). The main cause to employ COMSOL Multiphysics 6.0 due to its capabilities to coupling the heat transfer, conduction and fluid flow that it be necessity in simulating the microchannel heat sink. In addition, due to the varying temperature of fluid flow in microchannel heat sink COMSOL with FEM approach can take this problem in consideration and this point is principal for predicting the performance the heat transfer in MCHS with accurate results. The heat sink comprises multiple microchannels, and to streamline the computational process and reduce the number of grids, a single branch of the microchannel is analyzed as the computational domain to efficiently obtain results. Figure 1 provides a visual representation of the computational domains for all types of microchannels, as seen in their front view. Subfigures (a)–(d) illustrate the computational domains for rectangular microchannel (RMCH), rectangular microchannel with side rectangular grooves (RMCH-WSRG), converging microchannel (CMCHS) and converging microchannel with side rectangular grooves (CMCH-WSRG), respectively. Detailed dimensions are outlined in Table 1.

Boundary conditions

Assuming laminar and steady-state fluid flow, the continuity and momentum equations are employed with specific boundary conditions. For the microchannel, the following conditions are considered:

1. Inlet conditions are determined by the velocity, contingent upon the Reynolds number ranging from 200 to 1000.
2. The outlet condition is defined by static pressure and set to zero.
3. The walls of the microchannel heat sink (MCHS) are set to a no-slip condition.

On the other hand, the energy equation is formulated with the following boundary conditions:

1. The inlet condition is determined by tin and set to 293 K.
2. Symmetrical boundary conditions are applied to the left and right sides of the microchannel.
3. The bottom of the microchannels is subjected to a heat flux of 100 W cm^{-2}, simulating the heat source from a CPU chip.
4. The top of the MCHS is set as adiabatic.

Mesh dependency (MD)

The results of any model are influenced by the grid or mesh, necessitating a check for mesh dependency (MD). Mesh dependency is a method employed to assess the impact of the number of nodes or grids on result accuracy. This is achieved by calculating the value of any variable using different numbers of nodes or mesh types and determining the error percentage between two successive iterations. If the error percentage is small, it indicates that results can be reliably obtained within that range of nodes.

In this study, the maximum temperature in the fluid domain of the microchannel heat sink (MCHS) at Re = 600 was chosen as a variable parameter affected by the number of elements. We provide nine types of element sizes, including fine, finer, extra finer, extremely finer, normal, coarse, coarser, extra coarser and extremely coarser. Table 2 presents one case (CMWSR) as an example of the element sizes considered in this study. The element size labeled as "fine" (4046046 elements) was selected as the base mesh, as it exhibited only a 0.2% difference in maximum temperature compared to the highest mesh, labeled as "finer" (11425765 elements). Figure 2 provides a visual representation and further clarification.

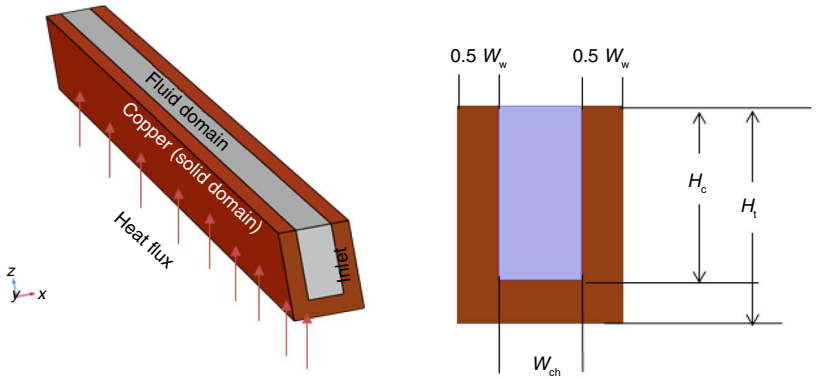

(a) Rectangular MCHS (RMCH) with its front view of inlet

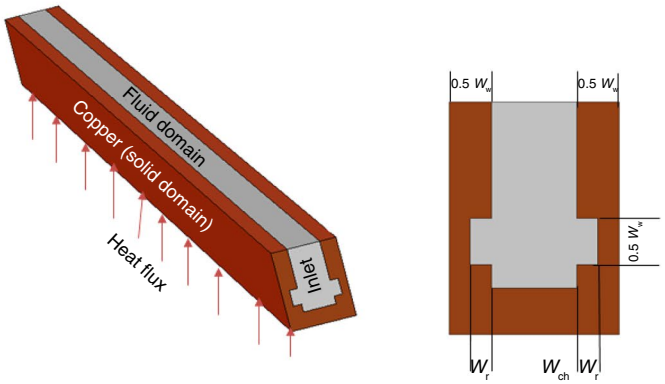

(b) RMCH-WSRG with its front view

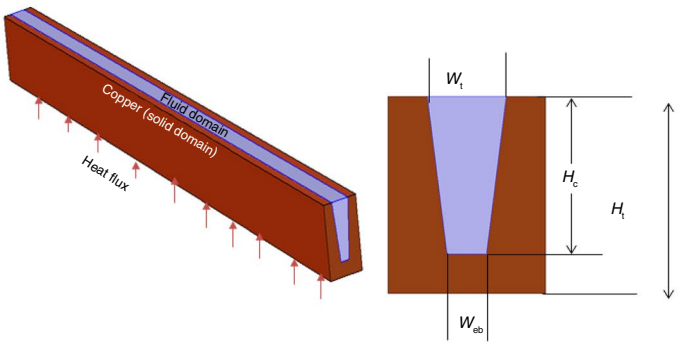

(c) CMCHS with its front view

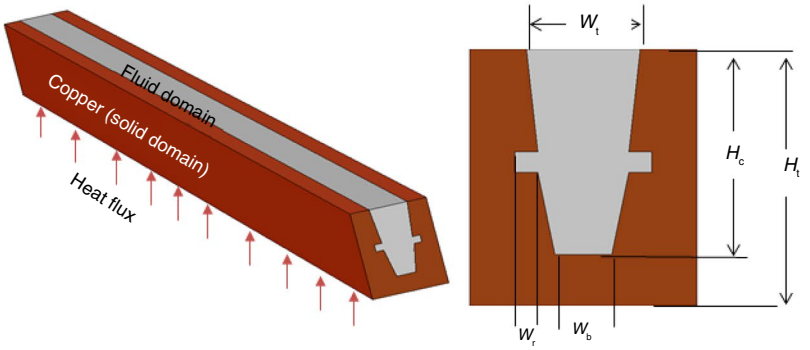

(d) CMCH-WSRG with its front view

Fig. 1 Geometrical configurations of MCHS with its front view **a** RMCH, **b** RMCH-WSRG, **c** CMCHS and **d** CMCH-WSRG

Table 1 MCHS dimensions [mm] used in the present work

Type	H_C	W_C	H_t	W_r	W_t	W_b
RMCH	0.4	0.2	0.5	–	–	–
RMCHS-WSRG	0.4	0.2	0.5	0.1	–	–
CMCHS	0.4	–	0.5	–	0.2	0.15
CMCHS-WSRG	0.4	–	0.5	0.1	0.2	0.15

Table 2 Mesh independence effect on maximum temperature

Element size	Element no.	AEQ	Temperature/K
Extremely coarse	124728	0.5471	300.98
Extra coarse	226010	0.5714	306.87
Coarser	433376	0.613	309.5
Coarse	902921	0.6378	312.8
Normal	1678275	0.6532	315.19
Fine	4046046	0.6726	321.65
Finer	11425765	0.6746	322.01

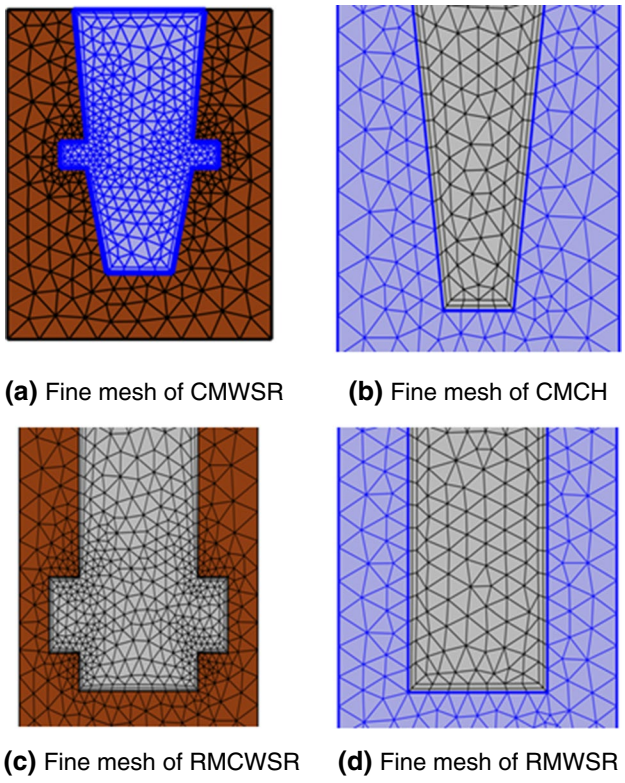

(a) Fine mesh of CMWSR **(b)** Fine mesh of CMCH

(c) Fine mesh of RMCWSR **(d)** Fine mesh of RMWSR

Fig. 2 Mesh distribution for different MCHS configurations

Results and discussion

A numerical investigation into the hydrothermal performance was conducted for all the microchannel heat sinks (MCHSs) under consideration. The bottom surface of the substrate was subjected to a heat flux of 100 W.cm^{-2}. The corresponding Reynolds numbers were specified as 200, 400, 600, 800 and 1000 for RMCH, RMCHS-WSRG, CMCHS and CMCHS-WSRG, respectively. Ag/H_2O nanofluid has been used as cooling liquid in the present because it has been proved to exhibit higher thermal conductivity and chemical stability compared with others type. These properties are more important to obtain higher heat transfer enhancement, where the heat transfer is related to thermal conductivity and the stability of nanofluids. Table 3 shows the thermophysical properties of both Ag and H_2O. The initial temperature of the coolant liquid (Ag/H_2O) was assumed to be 20 °C (293.15 K), and the volume fraction of nanoparticles varied between 0, 2.5, 5 and 7.5%. This study aims to explore hydrothermal performance to identify optimal designs that yield higher performance factors. The flowchart depicted in Fig. 3 outlines the main designs that will be numerically predicted in this investigation.

Table 3 Thermophysical of Ag and H_2O [35]

Property	Ag	Distilled water
Density / kg m^{-3}	10,500	997.1
Specific heat / J kg^{-1} K^{-1}	235	4179
Thermal conductivity / W m^{-1} K^{-1}	429	0.613

Figure 4 shows the conjugated heat transfer area and hydraulic diameter were calculated for all configurations of MCHS. The effect of little difference in both conjugated heat transfer area and hydraulic diameter due to the addition of rectangular grooves on both sides of models will be studied in the present work.

Model validation

To ensure the credibility of our results in this study, the numerical results obtained underwent validation against the findings of established researchers. This validation process involved comparing results related to pressure contour, velocity contour, temperature contour, Nusselt number, thermal resistance and other relevant parameters.

One of the initial validations was conducted with Feng et al. [33], wherein velocity contour and secondary flow field data for a rectangular microchannel heat sink were examined. The validation utilized the finite volume. The study

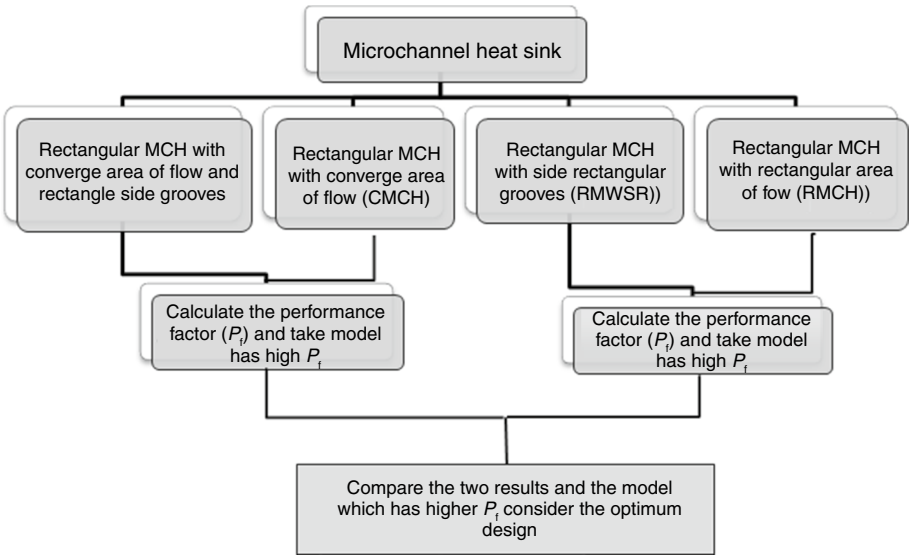

Fig. 3 Flowchart of optimizing the microchannel heat sink

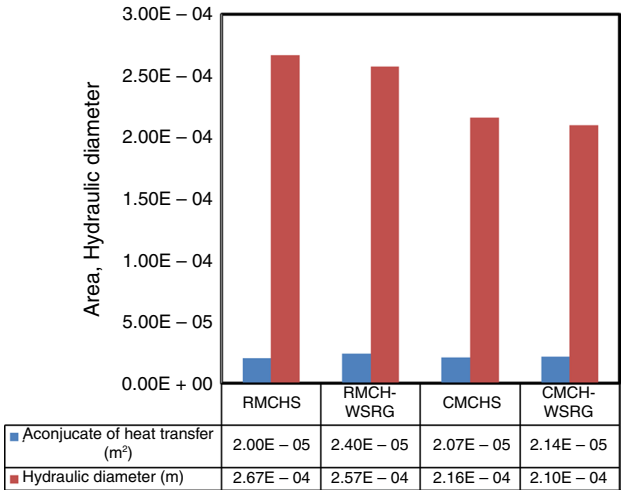

Fig. 4 Conjugate heat transfer area and hydraulic diameter

focused on water as the working fluid under steady-state conditions, with constant heat flux supplied at the microchannel's bottom. Figure 5 is generated, depicting velocity contours and temperature distribution at a specific cross section (axial location x/L = 0.625) under conditions of Re = 663 and a heat flux of 400 kW m^{-2}. These results were compared with the present simulation, which employed the finite element. The comparison revealed a notable agreement between the two simulations, with minimal discrepancies in velocity and temperature levels, attributed to the inherent differences in the utilized software platforms.

Figure 6a presents the validation of the local wall temperature for the heat sink in the current study, comparing the results with those obtained by Feng et al. [33]. The depiction in this figure illustrates that the wall temperature of the heat sink exhibits an increase from the inlet to the outlet. Notably, there is a consistent agreement between the outcomes of the present study and the findings reported by Feng et al. [33]. Additionally, Fig. 6b shows the validation of the friction factor for fluid flow at various Reynolds numbers along the rectangular microchannel. This figure highlights that the friction factor diminishes with an increase in the Reynolds number. The results presented in these figures demonstrate a substantial concordance between the outcomes of the present study and by Feng et al. [33].

In Fig. 7, a comparison is presented between the results obtained from our simulation and the theoretical findings by Qu et al. [1]. The illustration indicates that the disparity between our simulation outcomes and the theoretical results is below 10% for the inlet thermal resistance. This suggests that our code can be employed with increased confidence based on the favorable agreement observed.

Rectangular microchannel (RMCH) and rectangular microchannel with side rectangular grooves (RMWSR)

In energy management systems, an elevated pressure drop is often viewed as a drawback due to the associated higher pumping costs needed for efficient heat transfer. Therefore, it is recommended to utilize coolants with low ΔP characteristics and high thermal properties to meet system requirements effectively. It is well known that frictional drag causes a continuous decrease in pressure along the main flow direction. Figure 8 illustrates the pressure drop along the microchannel concerning the Reynolds number at various volume fractions for a rectangular microchannel heat sink (MCHS).

Observations from this figure suggest that an increase in Reynolds number results in a higher pressure drop. This

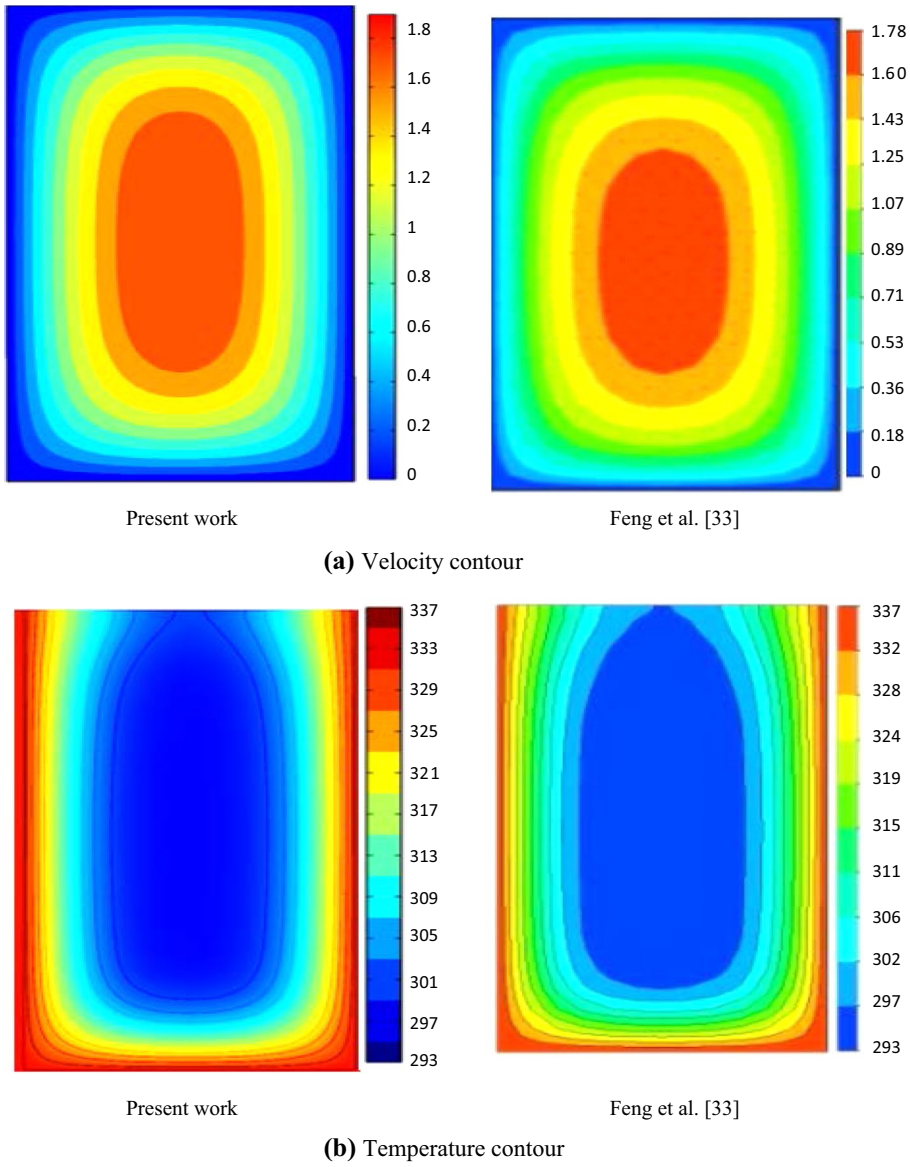

Fig. 5 Validation of present work **a** velocity and **b** temperature contours on a cross section (x/L = 0.625) in microchannel at Re = 663 with Feng et al. [33]

(a) Velocity contour

(b) Temperature contour

can be attributed to the corresponding increase in Reynolds number, indicating a rise in inlet velocity, while other properties such as fluid density, hydraulic diameter and viscosity remain constant in the case of incompressible and steady-state fluid flow. On the flip side, an increase in volume fraction (ϕ) leads to a heightened pressure drop, attributed to the increased viscosity of nanofluids with a rising volume fraction of nanoparticles. Despite the augmented pressure drop, the use of nanofluids as coolant liquids can be considered advantageous due to their improved heat transfer capabilities resulting from increased thermal conductivity.

On the flip side, the impact of varying nanofluid volume fractions on pressure drop at different Reynolds numbers for RMWSR is illustrated in Fig. 9. The figure demonstrates a consistent trend in the relationship between pressure drop and Reynolds number for different volume fractions, similar to the pattern observed in RMCH under the same conditions. The increasing volume fraction of nanofluid leads to the increase in the viscosity of nanofluid and hence the pressure drops as shown in Fig. 9, thereby demanding higher pumping power to pump the fluid.

To assess the influence of geometry on pressure drop and select the model with a lower pressure drop, the variation of pressure drop with Reynolds number for the two models (RMCH and RMCH-WSRG) is presented in Fig. 10 at a volume fraction of nanofluid equal to 7.5% and Re = 600. Figure 10 suggests that the RMCH-WSRG model experiences a slightly higher pressure drop compared to the RMCH model. This behavior can be attributed to that pressure drop in microchannel heat sink which is greatly affected by the ratio of the surface area to cross-sectional area, where the increasing this ratio led to an increase in the pressure drop.

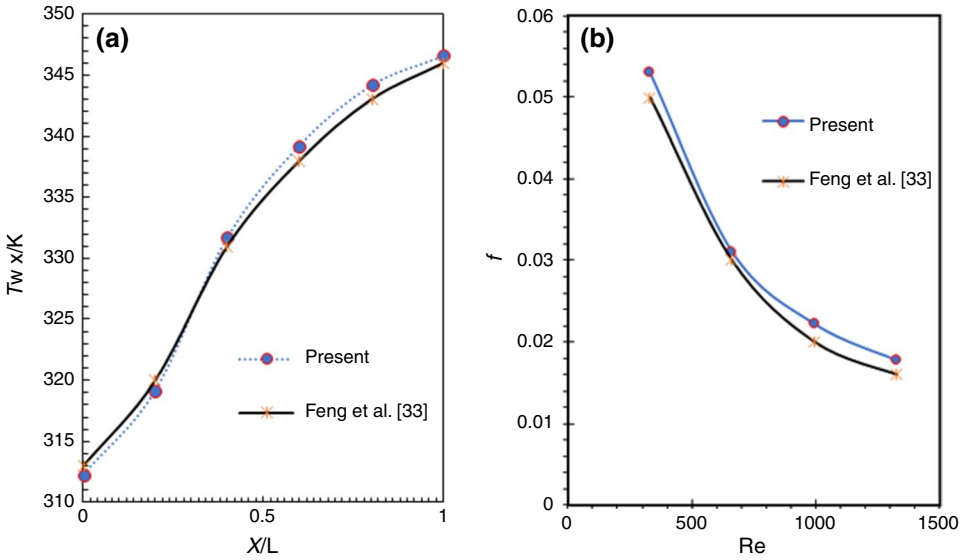

Fig. 6 Validation of the present results with the numerical results obtained by Feng et al. [33] for **a** local temperature of heat sink base with dimensionless x/L at Re = 663 **b** Friction factor vs. Re

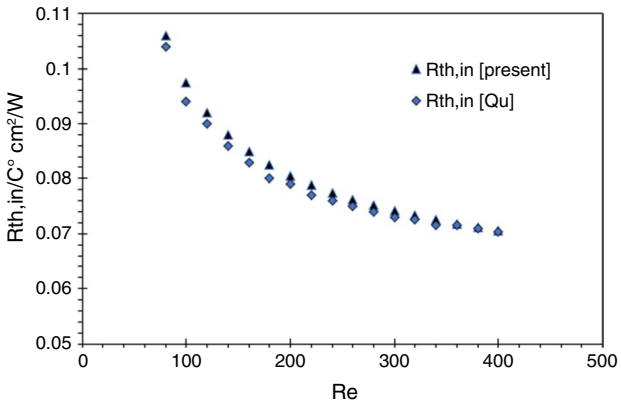

Fig. 7 Comparison of present results of inlet thermal resistance with that of Qu et al. [1] work

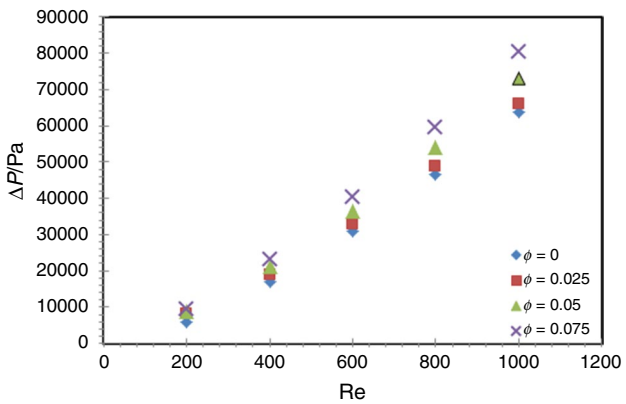

Fig. 8 Pressure drops v/s Re for RMCHS at different volume concentrations

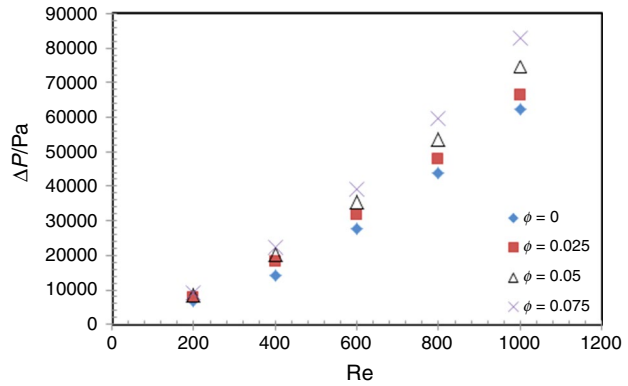

Fig. 9 Pressure drops v/s Re for RMCH-WSRG at different volume concentrations

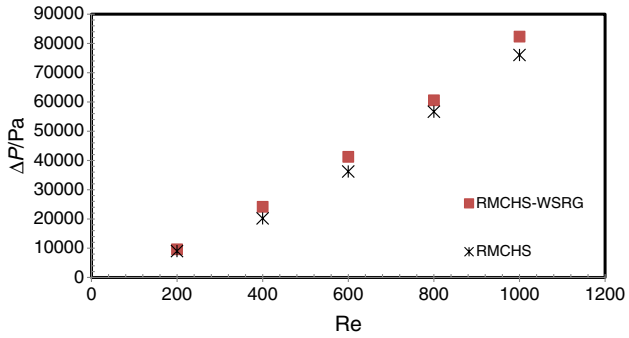

Fig. 10 Variations of pressure drops v/s Re for RMCH and RMWSR at a nanofluid volume fraction of 7.5%

Hence, an addition of small structures leads to an increase in this ratio; therefore, the frictional losses increase the pressure drop. To illustrate the impact of geometry on pressure

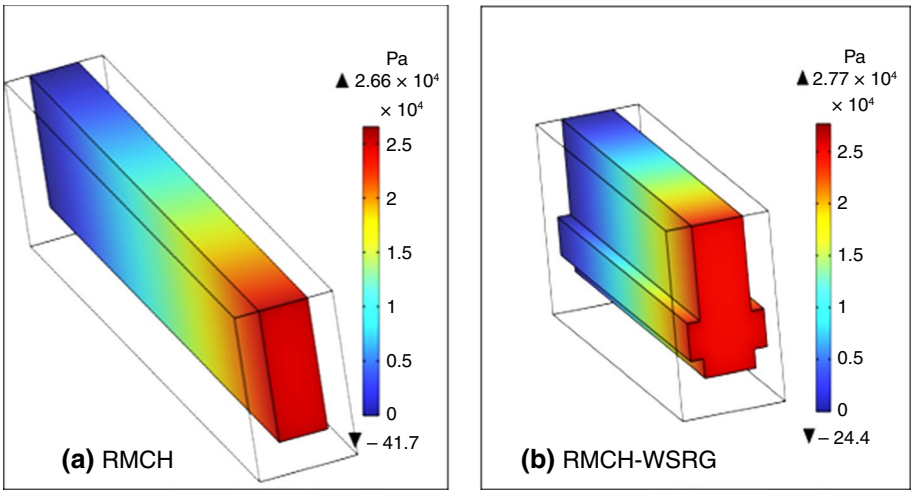

Fig. 11 Distribution of pressure contours for **a** RMCH and **b** RMCHS-WSRG

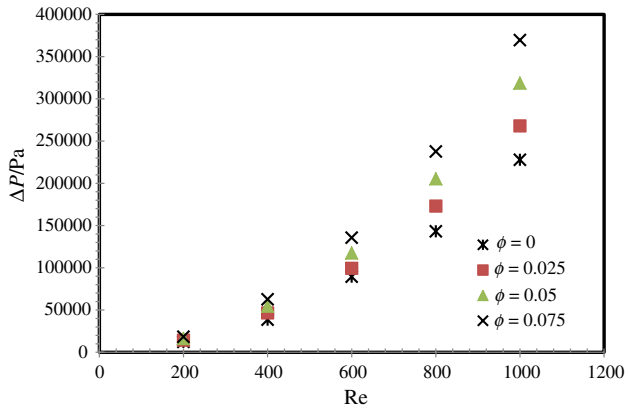

Fig. 12 Variation of pressure drops with Re at different volume fractions for CMCHS

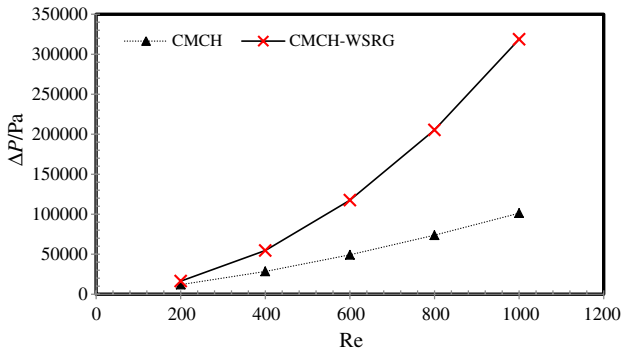

Fig. 13 Variation of pressure drop with Re for CMWSR and CMCHS at $\phi = 5\%$

distribution, Fig. 11a, b depicts the pressure distribution contours in RMCH and RMCHS-WSRG, respectively, at Re = 600 with a 7.5% volume fraction of nanoparticles. It can be stated that the limitation of RMCH-WSRG is higher pressure drop at all volume concertation of nanofluid compared to RMCHS, so it demands pump system with higher power.

Converge microchannel (CMCHS) and converge microchannel with side rectangular grooves (CMWSR)

In general, the influence of the percentage of volume fraction of nanoparticles on pressure drop results in an overall increase, as elucidated in Fig. 12. The impact of geometric configurations, specifically CMCHS and CMWSR grooves at a 5% volume fraction, is examined in Fig. 13. The findings from this figure suggest that the pressure drop in CMCHS-WSRG is slightly higher than in CMCH. This difference can be attributed to the addition of side rectangular grooves that lead to the increase in the ratio of surface area to cross section; in addition, it decreases the hydraulic diameter which leads to the low flow area. These conditions helped to increase the frictional losses and hence increase the pressure drop. The pressure distribution for both models is illustrated in Fig. 14 for further analysis. So it is necessary to keep the flow area at suitable range.

Figure 15 displays the velocity distribution in five planes (XZ) perpendicular to the main flow with a 7.5 vol% nanofluid at Re = 600 for (a) RMCH, (b) RMCH-WSR grooves, (c) CMCHS and (d) CMCHS-WSRG grooves. The velocity distribution within the microchannel heat sink featuring side rectangular grooves indicates a lateral shift followed by a return to the center of the flow. Notably, CMCHS-WSRG exhibits higher velocity distributions at the same Re value, density and dynamic viscosity. This observation can be attributed to the channel flow's shape and the hydraulic diameter, as depicted in Fig. 3. The figure illustrates that CMCH-WSRG have a smaller hydraulic diameter compared to other types. It

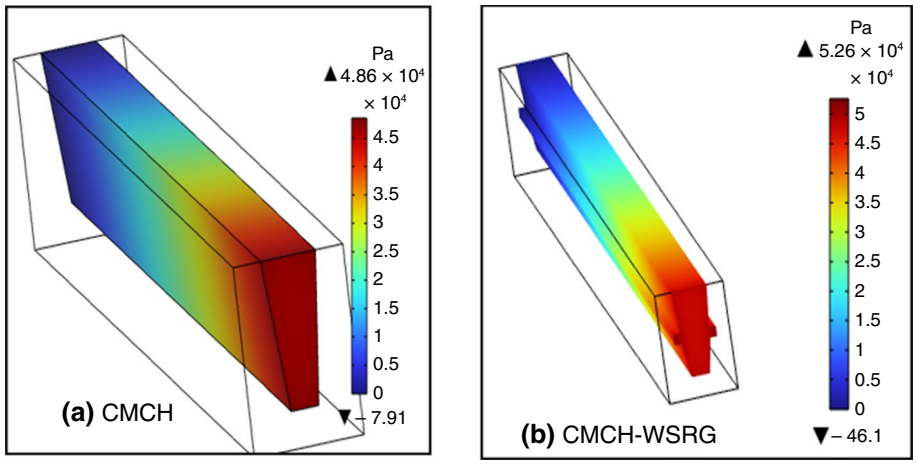

Fig. 14 Distribution of pressure contours in **a** CMCHS and **b** CMCHS-WSRG

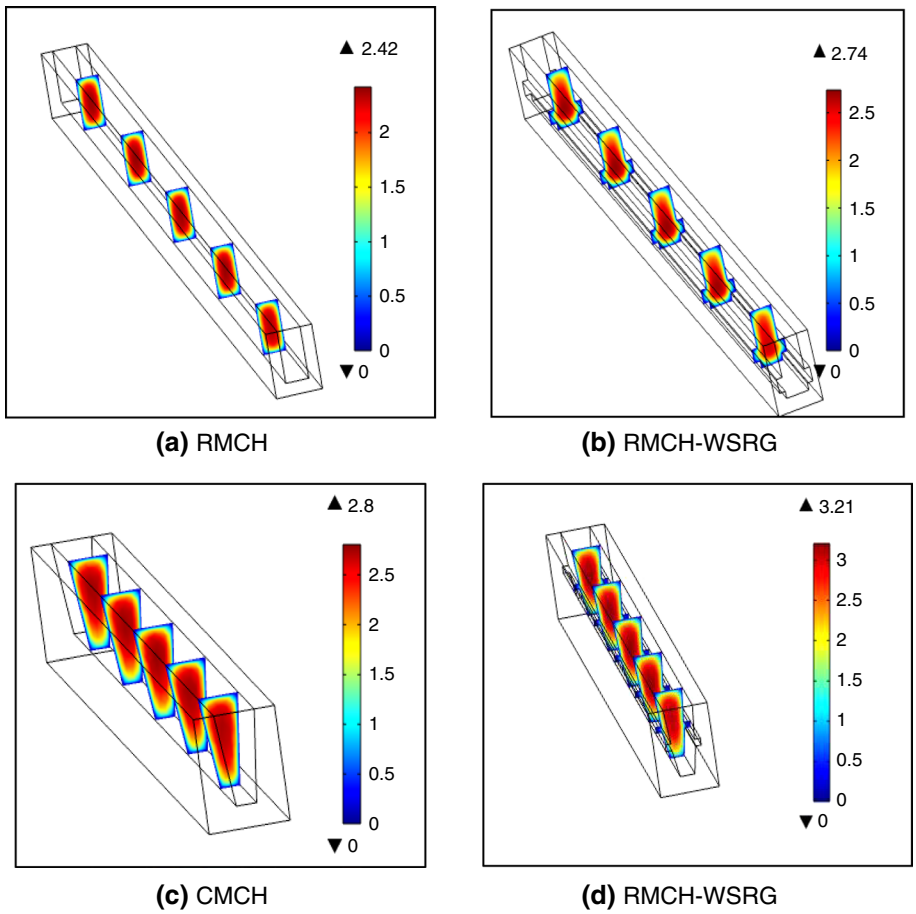

Fig. 15 Velocity distribution contour at five (XZ) **a** RMCH **b** RMCHS-WSRG at Re = 600 **c** CMCHS **d** CMCHS-WSRG

can be stated the increasing of velocity in CMCH-WSRG can lead to an increase in the pressure drop inside the microchannels. This increase in the pressure drop means loss in energy due to the fluid friction that flow through channels. Hence, many considerations must be taken in design the MCHS and choosing the appropriate cooling liquid due to the velocity of cooling is higher effected by thermophysical properties.

Thermal performance for different microchannel configurations

The thermal performance of the MCHS serves as a connecting factor between Nu (Nusselt number) and friction coefficient. To assess the thermal performance of the RMCH and RMCHS-WSRG models, Nu has been computed at various values of Reynolds number (Re) and

volume fractions of nanoparticles. Figure 16a, b depicts the relationship between Nu and Re for RMCH and RMCHS-WSR, respectively, while Fig. 17a, b illustrates Nu with Re for CMCHS and CMCHS-WSRG, respectively. In general, Nu increases with a rise in the volume fraction of the nanofluid. Moreover, for both models, Nu numbers show an increase with rising Re, indicating that higher Re numbers lead to enhanced heat transfer. This enhancement is attributed to the reduction in fluid temperature within the microchannel at higher Re values, facilitating efficient heat dissipation, as demonstrated in Fig. 15a, b, c and d for RMCH, RMCHS-WSRG, CMCHS and CMCHS-WSRG, respectively.

Average base temperature of a microchannel heat sink is very important and has more effect on the thermal performance of heat sink, and this can be attributed to that the base of heat sink attached directly to the integrated circuits and its temperature must be maintained within a certain limit. Where the higher temperature will lead to thermal stresses that will be affected on the reliability and efficiency of thermal system, so will cause reduction in the life of electronic equipment.

Hence, Fig. 18a, b, c and d shows the relation between the average base temperature for RMCH, RMCHS-WSRG, CMCHS and CMCHS-WSRG, respectively, with Reynolds number at different volume fractions of nanofluid. It can be

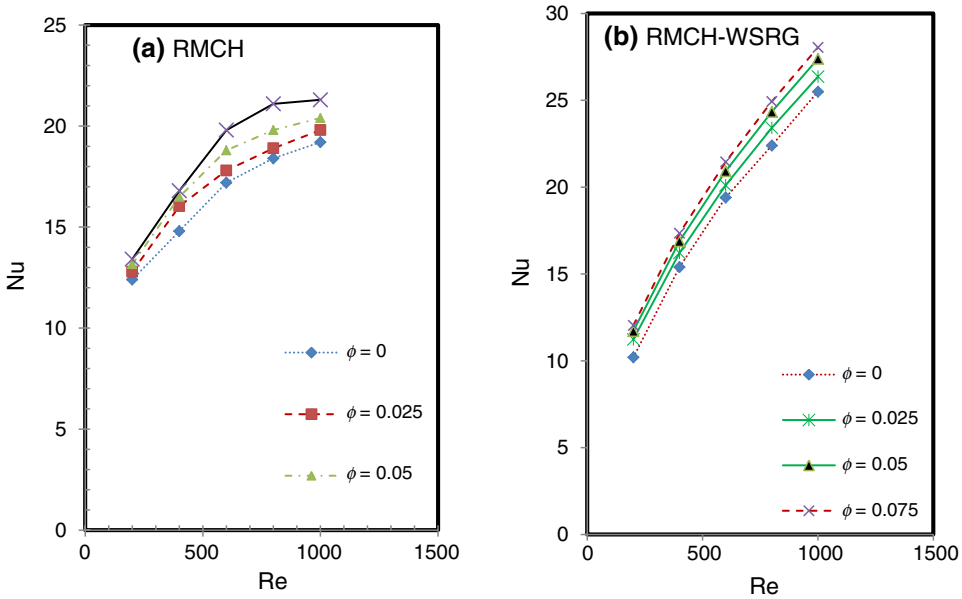

Fig. 16 Average Nusselt number vs. Reynolds number for **a** RMCHS and **b** RMCHS-WSRG

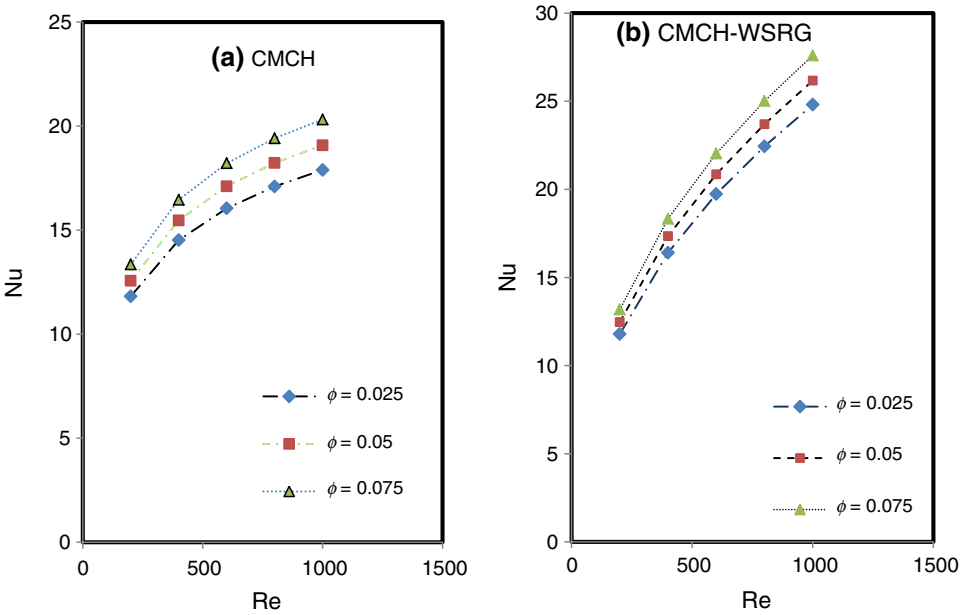

Fig. 17 Average Nusselt number v/s Re at different volume concentrations **a** CMCHS **b** CMCHS-WSRG grooves

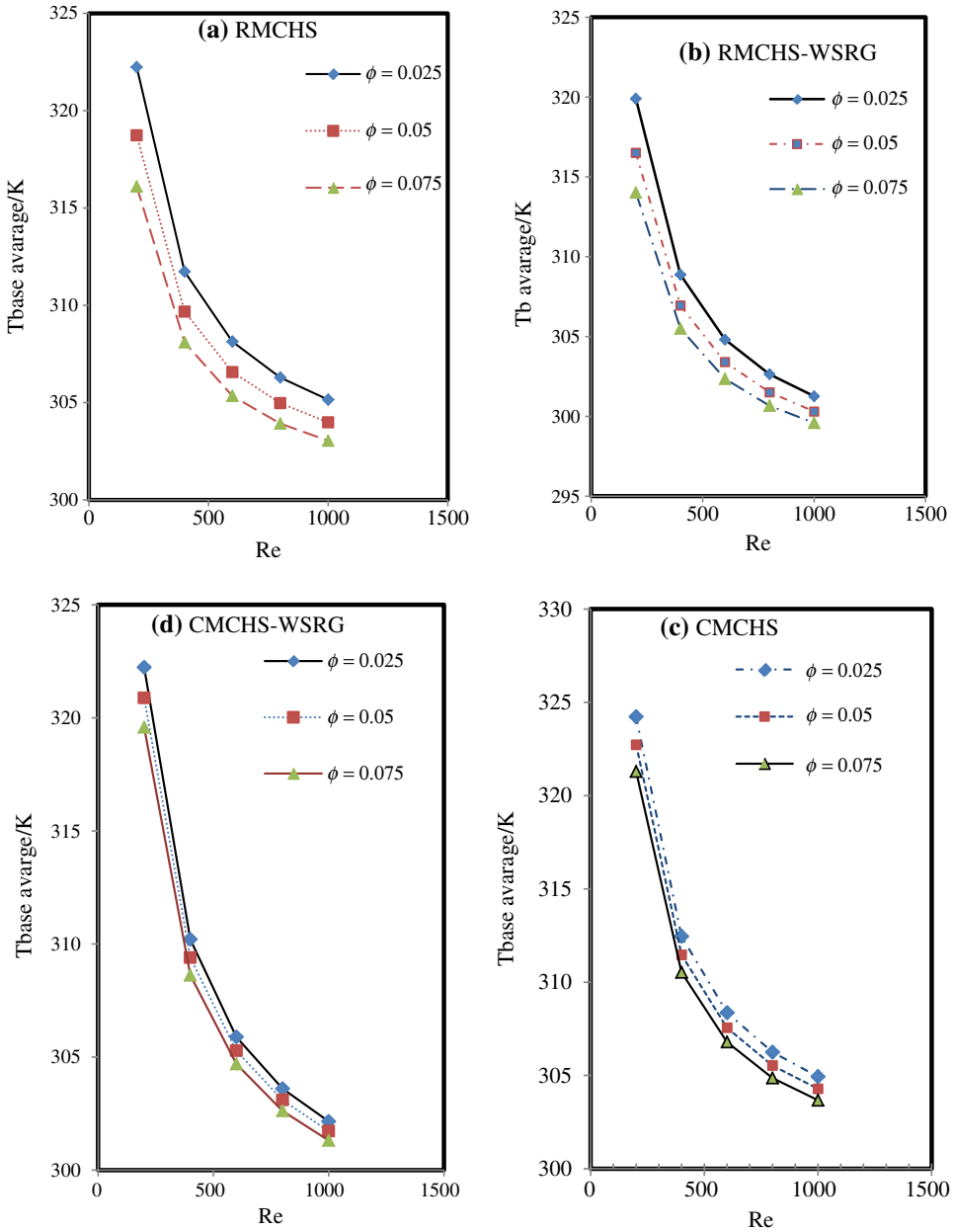

Fig. 18 Average temperature at the base of MCHS types v/s Re at different volume fractions of nanofluid

clear from these figures that the average base temperature of the four models of microchannel heat sink decreases as the volume fraction of the nanofluid increases. This decrease is attributed to the increase in thermal conductivity of the liquid with a higher volume concentration of nanoparticles which lead to dissipate higher heat transfer.

To demonstrate the impact of model configuration across all the types examined in this study, Fig. 19 provides a comparison of temperatures at the base of the MCHS for all models with a 5 vol% volume fraction of nanoparticles. The microchannels are arranged in descending order of temperature from high to low, specifically CMCHS, CMCHS-WSRG, RMCH and RMCHS-WSRG. This trend can be explained by the application of heat flux at the base of the microchannel, with the base area being consistent across all models. The observed temperature variation is influenced by the hydraulic diameter and conjugated area, where the conjugated area decreases from larger to smaller, as illustrated in Fig. 3 for RMCHS-WSRG grooves, CMCHS-WSRG, RMCH and CMCHS, respectively.

The temperature distribution contour depicted in Fig. 20 illustrates the temperature variations of four models at a Reynolds number of 600. The fluid temperature increases in the direction of flow. Generally, there are two methods for heat removal: One involves rapid heat transfer into the coolant through the channel's bottom surface, while the other entails initial upward conduction of heat through the channel wall before convective heat transfer occurs. Notably, the

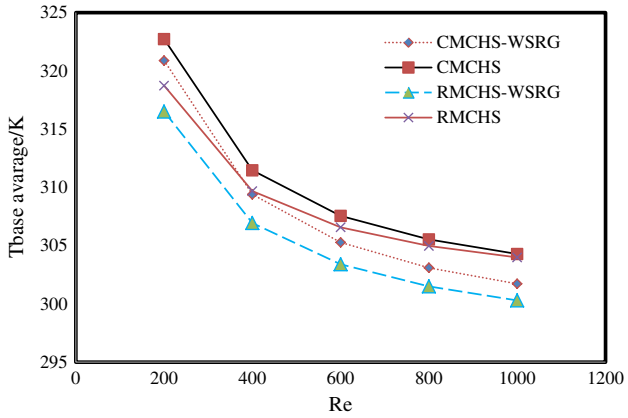

Fig. 19 Average base temperatures, Re for different types of MCHS at ∅ = 0.05

temperature distribution in RMCHS-WSRG grooves is comparatively smaller than in other types. This phenomenon can be attributed to the periodic disruption of thermal boundary layers and the presence of vortices at corners, facilitating heat extraction from the walls. Additionally, heat transportation is enhanced by the higher fluid occupancy in RMCHS-WSRG grooves compared to other types.

In summary, the hydrothermal properties, encompassing pressure drop and temperature play a crucial role in determining the overall performance of a microchannel heat sink. Consequently, the hydrothermal performance factor (PF), which can be considered as the ratio between Nusselt number ratio and friction coefficient ratio power of third. Hydrothermal performance factor is an indication to effectiveness of thermal with respect to pressure drop. Hence, if the value of hydrothermal performance exceeds 1, it means that the thermal performance is superior over pressure drop, and it becomes opposite if its value is less than 1. PF is governed by the formulawhere the symbol (o) denotes the original

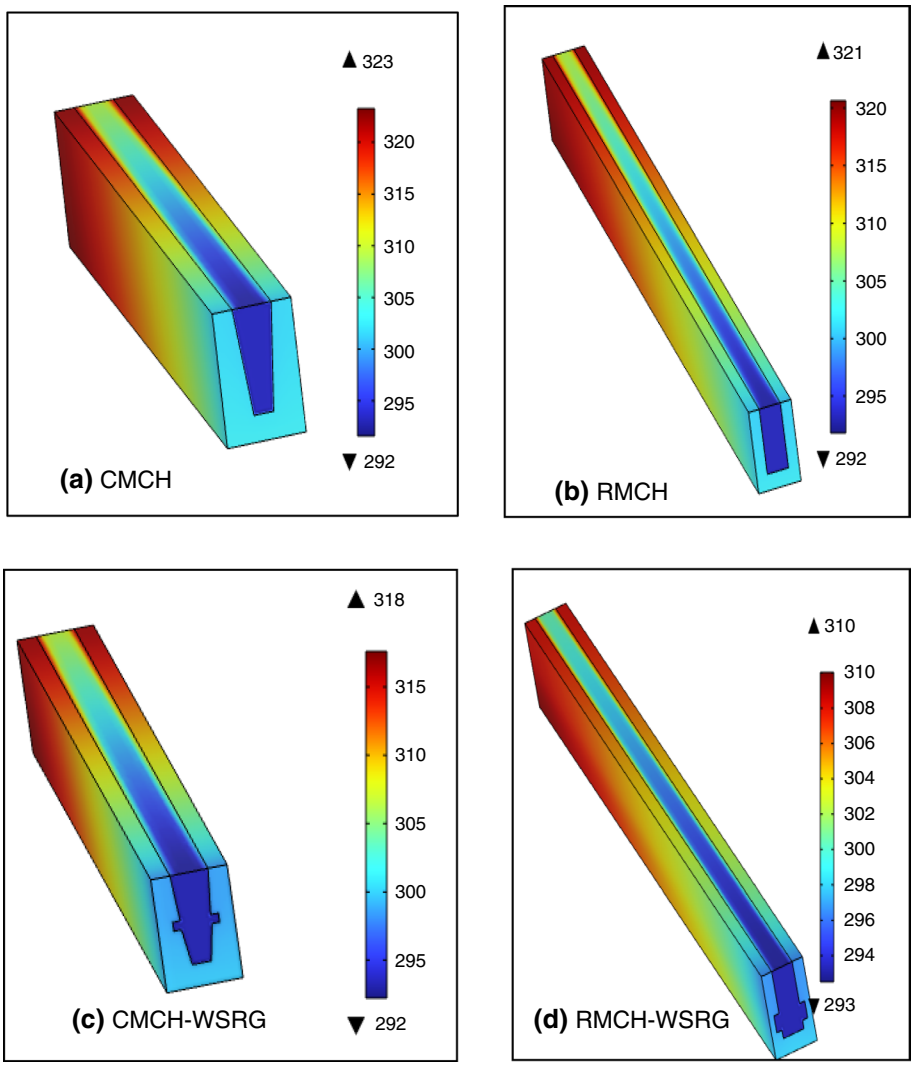

Fig. 20 Temperature contour at Re = 600 and 7.5% nanofluid volume fraction for **a** CMCHS, **b** RMCHS, **c** CMCHS-WSRG, **d** RMCHS-WSRG

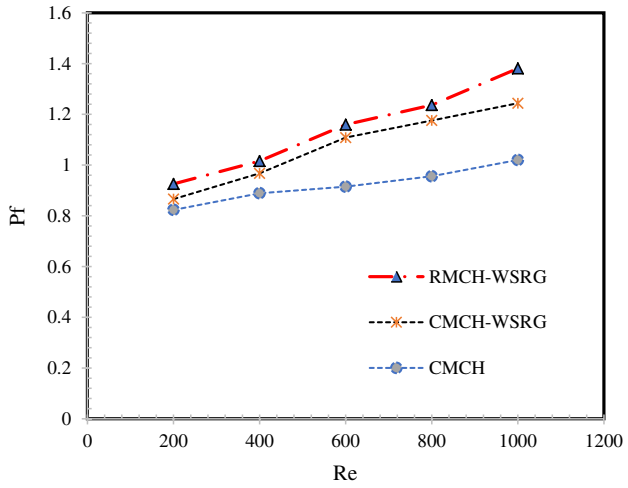

Fig. 21 Performance factor vs Re for different models

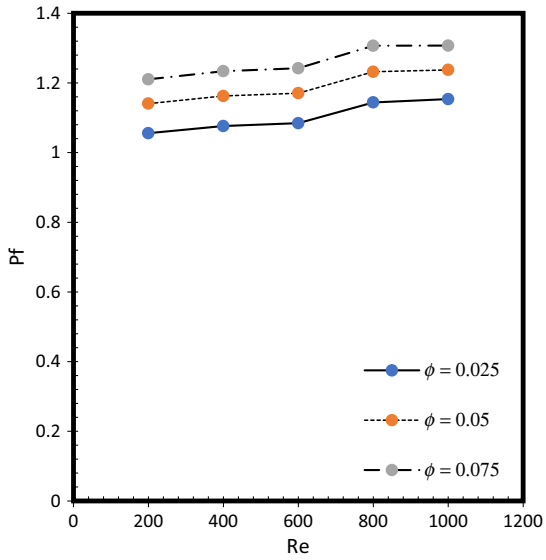

Fig. 22 Performance factor vs Re at different volume fractions of nanoparticles

shape (RMCH) and New indicates the shapes of (CMCHS, CMCHS-WSRG and RMCHS-WSRG). Performance factor is illustrated in Fig. 21 for the three models concerning (RMCH) as a reference. Notably, the performance factor of RMCHS-WSRG is slightly higher than CMCH-WSRG and CMCHS at low Reynolds number and began to increase more with a high Reynolds number. This discrepancy can be elucidated by the higher Nusselt number in RMCH-WSRG compared to the other configurations that resulted from the higher surface area of CMCH-WSRG which allowed to heat exchange for more time. Additionally, it is observed that the performance factor increases with the Reynolds number for all models, which is due to the increase in the velocity of fluid in MCHS that significantly affects the thermal performance. So as the velocities becomes higher, the rate of heat transfer from microchannel wall to the fluid will be increased. Also the increasing velocity will enhance the mixing process and reduce thermal boundary layer that allowed more performance heat exchange.

Effect of nanofluid on the performance factor

The computation of the performance factor, considering the impact of the volume fraction of nanoparticles in the nanofluid, is depicted in Fig. 22 specifically for the (RMCH-WSRG) configuration, which exhibits a high-performance factor. This figure shows that as the Reynolds number increases, the performance factor also increases. This phenomenon is attributed to the increase in velocity that accompanies an increase in the rate of heat exchange between the solid wall of the MCHS and the liquid, hence this inverse effect on the Nusselt number, establishing thermal performance as the controlling factor for the performance factor. Also, the findings of this figure stated that the increase in the volume fraction of Ag/H_2O nanofluid (0.025–0.075) can enhance the thermal performance of microchannel heat sink that resulted from the enhancement of the thermal conductivity of cooling liquid. Higher thermal conductivity of nanofluid leads to higher heat dissipation of fluid flow, hence keeping the electronic system at allowable limit of temperature.

Conclusions

Thermal management system such as in the field of electronic products demands high attention in thermal management due to its failures that can cause overheating due to inefficient thermal design. In addition to that, there is a problem related to the hydraulic performance such as high pressure drops that occur along MCHS, and this problem is from the significant limitations where the higher pressure drops lead to an increase in the consumption of pumping power; hence, the risk of leakage increases.

The main findings of the current study can be summarized as follows:

- Implementation of side rectangular grooves in both RMCH and CMCHS designs results in a significant increasing in fluid flow pressure drop, with the increase of 12.5 and 33.35%, respectively.
- The average temperature at the base of the heat sink is lower in the case of RMCH-WSRG compared to other groove types.
- Comparative analysis of the hydrothermal performance factor among the three models and the standard MCHS

(RMCHS) indicates that RMCH-WSRG exhibits superior hydrothermal performance due to their larger conjugated heated area.

- The utilization of CMCH-WSRG leads to a higher velocity distribution in comparison with other groove types, and this increase can lead to an increase in the heat transfer and fluid mixing and reduced thermal boundary layer.
- The performance factor increases with increasing volume fraction, which means using Ag/H2O improves the thermal performance of microchannel heat sink.
- With an increase in the Reynolds number, the performance factor rises, indicating an enhancement in performance. This can be attributed to the increased velocity associated with a rise in thermal effects, represented by the Nusselt number, where thermal performance becomes a controlling factor in the performance factor.

Acknowledgements The authors extend their appreciation to the Deanship of Research and Graduate Studies at King Khalid University for funding this work through Large Research Project under grant number RGP2/39/45.

References

1. Qu W, Ma C-D. Microchannel heat sinks: a review. Int J Heat Mass Transf. 2017;109:2381–416.
2. Kandlikar S. Heat transfer and fluid flow in minichannels and microchannels. Elsevier; 2006.
3. Lee PS, Garimella SV. Thermally developing flow and heat transfer in rectangular microchannels of different aspect ratios. Int J Heat Mass Transf. 2005;48:2041–51.
4. Sarviya RM, Fuskele V. Review on thermal conductivity of nanofluids. Mater Today Proc. 2017;4(2):4022–31.
5. Hung TC, Yan WM. Enhancement of thermal performance in a double-layered microchannel heat sink with nanofluids. Int J Heat Mass Transf. 2012;55(11–12):3225–38. https://doi.org/10.1016/j.ijheatmasstransfer.2012.02.057.
6. Ahmed MA, Shuaib NH, Yusoff MZ. Numerical investigations on the heat transfer enhancement in a wavy channel using nanofluid. Int J Heat Mass Transf. 2012;55(21–22):5891–8. https://doi.org/10.1016/j.ijheatmasstransfer.2012.05.086.
7. Wang XD, An B, Lin L, Lee DJ. Inverse geometric optimization for the geometry of nanofluid-cooled microchannel heat sink. Appl Therm Eng. 2013;55(1–2):87–94. https://doi.org/10.1016/j.applthermaleng.2013.03.010.
8. Kanti PK, Sharma KV, Minea AA, Kesti V. Experimental and computational determination of heat transfer, entropy generation and pressure drop under turbulent flow in a tube with fly ash-Cu hybrid nanofluid. Int J Therm Sci. 2021;167:107016.
9. Kanti P, Sharma KV, Said Z, Kesti V. Entropy generation and friction factor analysis of fly ash nanofluids flowing in a horizontal tube: experimental and numerical study. Int J Therm Sci. 2021;166:106972.
10 Kumar P, Alruqi M, Hanafi HA, Sharma P, Wanatasanappan VV. Effect of particle size on second law of thermodynamics analysis of Al_2O_3 nanofluid: application of XGBoost and gradient boosting regression for prognostic analysis. Int J Therm Sci. 2024;197:108825. https://doi.org/10.1016/j.ijthermalsci.2023.108825.
11. Sivakumar A, Alagumurthi N, Senthilvelan T. Experimental investigation of forced convective heat transfer performance in nanofluids of Al_2O_3/water and CuO/water in a serpentine shaped micro channel heat sink. Heat Mass Transf. 2015;52:1265–74.
12. Rostami J, Abbassi A. Conjugate heat transfer in a wavy microchannel using nanofluid by two-phase Eulerian-Lagrangian method. Adv Powder Technol. 2016;27:9–18.
13. Anbumeenakshi C, Thansekhar MR. On the effectiveness of a nanofluid cooled microchannel heat sink under non-uniform heating condition. Appl Therm Eng. 2017;113:1437–43.
14. Naphon P, Nakharintr L, Wiriyasart S. Continuous nanofluids jet impingement heat transfer and flow in a micro-channel heat sink. Int J Heat Mass Transf. 2018;126:924–32. https://doi.org/10.1016/j.ijheatmasstransfer.2018.05.101.
15. Ali M, Shoukat AA, Tariq HA, et al. Header design optimization of mini-channel heat sinks using CuO–H_2O and Al_2O_3–H_2O nanofluids for thermal management. Arab J Sci Eng. 2019;44:10327–38. https://doi.org/10.1007/s13369-019-04022-2.
16. Sajid MU, Ali HM, Sufyan A, et al. Experimental investigation of TiO_2–water nanofluid flow and heat transfer inside wavy mini-channel heat sinks. J Therm Anal Calorim. 2019;137:1279–94. https://doi.org/10.1007/s10973-019-08043-9.
17. Balaji T, Selvam C, Lal DM, et al. Enhanced heat transport behavior of micro channel heat sink with graphene based nanofluids. Int Commun Heat Mass Transf. 2020;117:104716. https://doi.org/10.1016/j.icheatmasstransfer.2020.104716.
18. Bazdar H, Toghraie D, Pourfattah F, et al. Numerical investigation of turbulent flow and heat transfer of nanofluid inside a wavy microchannel with different wavelengths. J Therm Anal Calorim. 2019;139:2365–80. https://doi.org/10.1007/s10973-019-08637-3.
19. Plant RD, Saghir MZ. Numerical and experimental investigation of high concentration aqueous alumina nanofluids in a two and three channel heat exchanger. Int J Thermofluids. 2021;9:100055. https://doi.org/10.1016/j.ijft.2020.100055.
20. Heidarshenas A, Azizi Z, Peyghambarzadeh SM, et al. Experimental investigation of heat transfer enhancement using ionic liquid-Al_2O_3 hybrid nanofluid in a cylindrical microchannel heat sink. Appl Therm Eng. 2021;191:116879. https://doi.org/10.1016/j.applthermaleng.2021.116879.
21. Nimmagadda R, Venkatasubbaiah K. Conjugate heat tranfer analysis of micro-channel using novel hybrid nanofluids (Al_2O_3 + Ag/Water). Eur J Mech B Fluids. 2015;52:19–27.
22. Abaszadeh M, Safavinejad A, Delouei AA, Amiri H. Analysis of radiative heat transfer in two-dimensional irregular geometries by developed immersed boundary–lattice Boltzmann method. J Quant Spectrosc Radiat Transf. 2022;280:108086. https://doi.org/10.1016/j.jqsrt.2022.108086.
23 Abaszadeh M, Safavinejad A, Amiri H, Delouei AA. A direct-forcing IB-LBM implementation for thermal radiation in irregular geometries. J Therm Anal Calorim. 2022;147(20):11169–81. https://doi.org/10.1007/s10973-022-11328-1.
24. Karimnejad S, Delouei AA, He F. Coupling immersed boundary and lattice Boltzmann method for modeling multi-body interactions subjected to pulsatile flow. Math Methods Appl Sci. 2023;46(6):6767–86. https://doi.org/10.1002/mma.8939.
25 AmiriDelouei A, Sajjadi H, Ahmadi G. The effect of piezoelectric transducer location on heat transfer enhancement of an ultrasonic-assisted liquid-cooled CPU radiator. Iran J Sci Technol Trans Mech Eng. 2023. https://doi.org/10.1007/s40997-023-00667-5.
26 Delouei AA, Naeimi H, Sajjadi H, Atashafrooz M, Imanparast M, Chamkha AJ. An active approach to heat transfer enhancement in indirect heaters of city gate stations: an experimental modeling. Appl Therm Eng. 2024;237:121795.
27. Akbari OA, Toghraie D, Karimipour A, Safaei MR, Goodarzi M, Alipour H, Dahari M. Investigation of rib's height effect on heat

transfer and flow parameters of laminar water–Al_2O_3 nanofluid in a rib-microchannel. Appl Math Comput. 2016;290:135–53.
28. Muhammad NMA, Sidik NAC, Saat A, Abdullahi B. Effect of nanofluids on heat transfer and pressure drop characteristics of diverging-converging minichannel heat sink. CFD Lett. 2019;11:105–20.
29. Bayat J, Nikseresht AH. Thermal performance and pressure drop analysis of nanofluids in turbulent forced convective flows. Int J Therm Sci. 2012;60:236–43.
30 Xuan Y, Roetzel W. Conceptions for heat transfer correlation of nanofluids. Int J Heat Mass Transf. 2000;43:3701–7. https://doi.org/10.1016/S0017-9310(99)00369-5.
31. Drew DA, Passman SL. Theory of multi component fluids. Berlin: Springer; 1999.
32. Aminossadati S, Ghasemi B. Natural convection cooling of a localised heat source at the bottom of a nanofluid-filled enclosure. Eur J Mech B Fluids. 2009;28(5):630–40.
33. Feng Z, Luo X, Guo F, Li H, Zhang J. Numerical investigation on laminar flow and heat transfer in rectangular microchannel heat sink with wire coil inserts. Appl Therm Eng. 2017;116:597–609.
34. Xu M, Lu H, Gong L, Chai JC, Duan X. Parametric numerical study of the flow and heat transfer in microchannel with dimples. Int Commun Heat Mass Transf. 2016;76:348–57.
35 Hadavand M, et al. A numerical investigation on the effects of mixed convection of Ag-water nanofluid inside a sim-circular lid-driven cavity on the temperature of an electronic silicon chip. Appl Therm Eng. 2019;162:114298.